Advantages of using gold hollow nanoshells in cancer photothermal therapy

Sattar Abbasi[1,†], Mojtaba Servatkhah[1,‡], and Mohammad Mehdi Keshtkar[2,§]

[1] *Department of Physics, Marvdasht Branch, Islamic Azad University, Marvdasht, Iran*
[2] *Department of Physics, Payame Noor University, P. O. Box* 19395–3697, *Tehran, Iran*

(Received 14 November 2015; revised manuscript received 29 February 2016; published online 25 June 2016)

Lots of studies have been conducted on the optical properties of gold nanoparticles in the first region of near infrared (650 nm–950 nm), however new findings show that the second region of near-infrared (1000 nm–1350 nm) penetrates to the deeper tissues of the human body. Therefore, using the above-mentioned region in photo-thermal therapy (PTT) of cancer will be more appropriate. In this paper, absorption efficiency is calculated for gold spherical and rod-shaped nanoshells by the finite element method (FEM). The results show that the surface plasmon frequency of these nanostructures is highly dependent on the dimension and thickness of shell and it can be adjusted to the second region of near-infrared. Thus, due to their optical tunability and their high absorption efficiency the hollow nanoshells are the most appropriate options for eradicating cancer tissues.

Keywords: surface plasmon, absorption efficiency, near-infrared, nanotubes

PACS: 73.20.Mf, 78.20.Ci, 87.50.wp, 78.67.Ch **DOI:** 10.1088/1674-1056/25/8/087301

1. Introduction

Cancer therapy has faced different challenges among which are the weaknesses of common treatment methods. Thus by using nanoparticles as a therapeutic agents provides a promising future for cancer treatment.[1–9] In the past few decades, photo-thermal therapy (PTT) has been studied widely to enhance cancer treatment efficiency.[10–27]

Some specific metallic nanoparticles that have unique optical features are called plasmonic nanoparticles.[28–32] The absorption efficiencies of these metals, including gold, copper, and silver, are improved due to localized surface plasmon resonance (SPR),[33–42] which is an aggregate oscillation of excited conduction electrons on the metal surface caused by strong interaction with incident light at a specific wavelength. SPR causes high absorption efficiency for plasmonic nanoparticles which can be adjusted by changing shape, size, and local refractive index.

Among all metallic nanoparticles, gold nanoparticles are used most extensively in cancer therapy due to their special optical properties particularly in infrared wavelengths.[43–55] Also, in comparison with that of any organic dye molecules the optimal absorption efficiency of gold nanoparticles is very conducive to cancer therapy. Furthermore, they are more appropriate candidates for cancer therapy due to their better biological compatibility and suitable integration with a variety of biomolecule ligands.[56–62]

Irradiation of electromagnetic light can cause excitation in tiny inorganic molecules which leads to heat generation. In this method inorganic molecules, specially gold nanoparticles, are used to absorb incident light and cause heat in the region.[63] This heat originates from the photon energy conversion and is enough to eradicate cancer cells which is a considerably non-invasive method. As such, restriction of using traditional thermal treatment in cancer therapy, which causes damage to adjacent tissue, is omitted by the PTT method.[64]

The appropriate size of gold nanoparticles should be less than 100 nm, because larger particles tend to have lower blood circulation half-life: they are rapidly cleared by the body system which is not optimal for specific targeting of tumor sites.[65] Besides, ideal gold nanoparticles which are suitable for cancer therapy, should have a larger cross section in the near-infrared region. Absorption cross section is an important factor to evaluate the influence of heat produced from the incident light.[66] The reason for choosing the near-infrared region is that absorption of light in healthy tissues is low while transmission of it is high.[67,68] However, the 650-nm to 950-nm wavelength range, which is called the first window of near-infrared, is not optimal due to background noise caused by tissue fluorescence and depth limitation of 1 cm to 2 cm.[69]

Recent studies have shown that the depth of penetration into the tissue reaches its maximum value in the second near-infrared window (1000 nm–1350 nm).[70] This feature is highly desirable for treating the tumors, which are deeper in the body.

†Corresponding author. E-mail: abbasi86@mail.com
‡E-mail: servatkhah@miau.ac.ir
§E-mail: keshtkar3@gmail.com

© 2016 Chinese Physical Society and IOP Publishing Ltd

Given that in recent years various metals like gold have been successfully synthesized in the form of hollow nanostructures,[71–83] in this paper, the optical properties of the hollow nanoshells are taken into account, and nanoshells with different core materials are compared with each other. Finally, the advantages of the hollow nanoshells over the other nanoshells are provided for cancer therapy.

2. Theory

Comparing the results from various techniques with simulated optical properties of nanoparticles can help us choose the best option. Some basic and advanced mathematical theories used to simulate scattering and absorption efficiencies of nanoparticles are described below.

2.1. Poynting vector and optical response of a single nanoparticle

The Poynting vector $\boldsymbol{S}$ represents the amount of power per unit area that a wave carries in the direction of its propagation. The time-averaged Poynting vector $\boldsymbol{S}_{\rm av}$ (units of W/m^2) is given by

$$\boldsymbol{S}_{\rm av} = \frac{1}{2}\Re\left(\boldsymbol{E}\times\boldsymbol{H}^*\right). \tag{1}$$

When light propagates in a medium it dissipates by interaction with charged particles (electrons and atomic nuclei) of the matter. The optical response of a single gold nanoparticle to incident light is characterized by its absorption and scattering cross section or the amount of energy absorbed by the nanoparticle (due to ohmic losses) and scattering per unit area. The absorption cross section $\sigma_{\rm abs}$ of a single gold nanoparticle can be given as a fraction of integrated resistive heating over the nanoparticle's volume V divided by the incident power density:

$$\sigma_{\rm abs} = \frac{2}{c_0\varepsilon_0 n E_{\rm inc}^2}\int \Re\left(\sigma\boldsymbol{E}\cdot\boldsymbol{E}^* - {\rm i}\omega\boldsymbol{E}\cdot\boldsymbol{D}^*\right){\rm d}V, \tag{2}$$

where c_0, n, and $E_{\rm inc}$ are the speed of light in a vacuum, the refractive index of the medium and the magnitude of the incident electric field, respectively. The scattering cross section $\sigma_{\rm sca}$ on the other hand is a fraction of the outgoing electromagnetic energy flux over an arbitrary boundary S surrounding the gold nanoparticle per the incident power density, and is given by

$$\sigma_{\rm sca} = \frac{2}{c_0\varepsilon_0 n E_{\rm inc}^2}\int \Re\left(\boldsymbol{E}_{\rm sca}\times\boldsymbol{H}_{\rm sca}^*\right){\rm d}S. \tag{3}$$

Absorption and scattering efficiencies are dimensionless quantities which are defined as follows:

$$Q_{\rm abs} = \frac{\sigma_{\rm abs}}{G}, \quad Q_{\rm sca} = \frac{\sigma_{\rm sca}}{G}, \tag{4}$$

where G is the particle cross sectional area projected onto a plane perpendicular to the incident beam (e.g., $G = \pi a^2$ for a sphere with radius a).

An extensive comparison has been provided previously among techniques used to simulate optical features of metallic nanostructures, especially gold nanoparticles. These techniques include Mie theory, the finite element method (FEM), discrete-dipole approximation (DDA), the transition matrix 'null-field' method (T-matrix), and the finite-difference time-domain (FDTD) method.[84]

2.2. Mie theory

Mie solution is widely used as a major theory of many prior studies done for studying the treatment of SPR. This theory is an analytical solution simulating the scattering of electromagnetic radiation by spherical particles in Maxwell's equations.[85–89]

By using Mie theory for homogeneous spheres $Q_{\rm sca}$ and $Q_{\rm ext}$ can be calculated for gold nanospheres. These efficiencies are infinite series as follows:

$$Q_{\rm ext} = \frac{2}{x^2}\sum_{n=1}^{\infty}(2n+1)\,{\rm Re}(a_n+b_n), \tag{5}$$

$$Q_{\rm sca} = \frac{2}{x^2}\sum_{n=1}^{\infty}(2n+1)\left(|a_n|^2+|b_n|^2\right), \tag{6}$$

$$Q_{\rm abs} = Q_{\rm ext} - Q_{\rm sca}, \tag{7}$$

$$a_n = \frac{m\psi_n(mx)\,\psi_n'(x) - \psi_n(x)\,y_n'(mx)}{m\psi_n(mx)\,\xi_n'(x) - m\xi_n(x)\,\psi_n'(mx)}, \tag{8}$$

$$b_n = \frac{\psi_n(mx)\,\psi_n'(x) - m\psi_n(x)\,\psi_n'(mx)}{\psi_n(mx)\,\xi_n'(x) - m\xi_n(x)\,\psi_n'(mx)}, \tag{9}$$

in which n is the refractive index of the sphere; n_m is the surrounding medium; n divided by n_m becomes m; ψ_n, and ξ_n are the Riccati–Bessel functions; the prime denotes the first differentiation with respect to the argument in parentheses; $2\pi n_m R/\lambda$ is the given value of the size parameter x.

Mie theory was presented more than 100 years ago. Since then it has been improved widely, but its limitations are significant. The main failure of solution for such an analytical method appears in non-spherical symmetric particles which makes it very limited. Besides, ignoring substrate interaction makes Mie theory more difficult to simulate many experiments.[90–92]

2.3. Finite element method

To obtain the optical properties of different shapes of nanostructures, a more comprehensive mathematical method, which does not have the complexity nor limitation of an analytical solution (Mie theory), is needed. The finite element method (FEM), which is an approximate solution of differential equations, is a powerful numerical solution. FEM is one of the most famous solutions in computational physics which

makes it feasible to achieve the optical features of nanostructures with different shapes.[93–95]

Simulations in this paper have been carried out by using the FEM. Water with a refractive index of 1.33, is considered as a context medium in which nanoparticles have been placed. Also, Johnson–Christy data for the dielectric function of a gold nanoparticle are used at different wavelengths.[96]

2.3.1. Boundary conditions in FEM

For a full mathematical description of a metal–dielectric interface with the Helmholtz equation (10), a set of boundary conditions (Eqs. (11)–(14)) should be taken into account for the discontinuity of the electrical and magnetic fields at the boundary between medium 1 and medium 2

$$\nabla \times \nabla \times \boldsymbol{E} - k_0^2 \tilde{\varepsilon} \boldsymbol{E} = 0, \tag{10}$$

$$\hat{n} \times (\boldsymbol{H}_1 - \boldsymbol{H}_2) = \boldsymbol{J}, \tag{11}$$

$$\hat{n} \times (\boldsymbol{E}_1 - \boldsymbol{E}_2) = 0, \tag{12}$$

$$\hat{n} \cdot (\boldsymbol{D}_1 - \boldsymbol{D}_2) = \rho, \tag{13}$$

$$\hat{n} \cdot (\boldsymbol{B}_1 - \boldsymbol{B}_2) = 0, \tag{14}$$

where $\hat{n}$, $k_0 = \omega\sqrt{\mu_0 \varepsilon_0}$, and $\tilde{\varepsilon}$ are the unit normal vector on the boundary, the wave number in a vaccum, and the electric permittivity of the medium respectively.

To truncate the computational domain a perfect electric conductor (PEC) equation (15), a perfect magnetic conductor (PMC) equation (16), and an absorbing boundary conductor (ABC) equation (17), are used as conditions:

$$\hat{n} \times \boldsymbol{E} = 0, \tag{15}$$

$$\hat{n} \times \boldsymbol{H} = 0, \tag{16}$$

and

$$\hat{n} \times \boldsymbol{H} = \frac{1}{\sqrt{\mu_0 \varepsilon_0}} \times \hat{n} \times \hat{n} \times \boldsymbol{E} + \hat{n} \times \boldsymbol{H}_{\text{inc}} - \frac{1}{\sqrt{\mu_0 \varepsilon_0}} \times \hat{n} \times \hat{n} \times \boldsymbol{E}_{\text{inc}}, \tag{17}$$

where $\boldsymbol{H}_{\text{inc}}$ and $\boldsymbol{E}_{\text{inc}}$ are the incident electric and magnetic fields, respectively.

2.3.2. An overview of the FEM

The finite element is a numerical technique that finds an approximate solution to a partial differential equation by decomposing it into a system of simpler equations. This method is widely used today to describe the behavior of an electromagnetic wave incident on an object with dielectric properties different from a surrounding medium. In FEM it is realized by solving the Maxwell equations (18) as a system with complex boundary conditions.

$$\nabla \times \boldsymbol{E} = -\frac{\partial \boldsymbol{B}}{\partial t}, \tag{18a}$$

$$\nabla \times \boldsymbol{H} = \frac{\partial \boldsymbol{D}}{\partial t} + \boldsymbol{J}, \tag{18b}$$

$$\nabla \boldsymbol{D} = \rho, \tag{18c}$$

$$\nabla \boldsymbol{B} = 0. \tag{18d}$$

To demonstrate the method, consider a homogeneous spatial domain Ω, where the time harmonic electric field is defined by the Helmhotz wave equation. This is a typical boundary-value problem that has a form

$$\mathscr{L}\phi = f = 0, \tag{19}$$

where $\mathscr{L} = \left(\nabla \times \nabla \times -k_0^2 \tilde{\varepsilon}\right)$ is a differential operator, $\phi = E$ is an unknown function to be computed in the region Ω, and f is a forcing term (or excitation). Boundary conditions that enclose domain Ω can be as simple as Neumann ($\boldsymbol{n}\nabla\phi = S$ where n is a normal vector and S is a scalar function) or Dirichlet conditions ($\phi = S$) or more impedance and radiation conditions. The computational domain Ω is divided into smaller elements, Ω_{e}, size of which depends on an expected variation of the unknown function. The solution for the unknown function ϕ within each element, is approximated by an expansion with a finite number of basic functions $\phi' \approx \sum_{i=1}^{N} c_i v_i$, where c_i are the unknown coefficients of the basis function v_i. The solution in this system of N equations, produces ϕ' that is a best fit to the unknown function. Variational formulation and weighted residual formulation are two well known methods to solve this problem and find coefficients.

The variational method,[97–99] also known as the Ritz method is based on formulating the boundary value problem (19) in terms of a functional. It can be shown for the case of self-joint and positive-definite operator L, the functional can be written in the form of

$$F_{\text{e}}(\phi') = \frac{1}{2}\int_{\Omega_{\text{e}}} \phi' \mathscr{L}\phi' \,\mathrm{d}\Omega - \int_{\Omega_{\text{e}}} f\phi' \,\mathrm{d}\Omega. \tag{20}$$

The minimization of the function $F_{\text{e}}(\phi')$, produces cofficients c_i so ϕ' is the best approximation to the solution.

The weighted residual method, is another way to find an approximation solution to Eq. (19). If a trial function ϕ' is an approximate solution to Eq. (19), then substitution of it into ϕ yields a nonzero residual $= \mathscr{L}\phi' - f \neq 0$. In order to obtain the best approximation of ϕ', residual r must be as small as possible at all locations in Ω_{e}. To force this condition test or weighting functions w_i (where i is the number of unknown degrees of freedom in the approximation), needs to be chosen so weighted residual integrals R_i

$$R_{\text{e}} = \int_{\Omega_{\text{e}}} w_i r \,\mathrm{d}\Omega = 0. \tag{21}$$

The guess coefficient will determine the accuracy of the found approximate solution to Eq. (19) within Ω_{e}. To summarize the FEM, in order to solve the problems defined by partial

differential equations (PDEs), the following steps should be taken:[100]

(i) discretize the computational domain Ω into smaller elements (triangle or tetrahedral for two-dimensional (2D) or three-dimensional (3D) space);

(ii) define an interpolation function;

(iii) for the element, assemble the system of equations by the use of the Ritz or weighted residual method;

(iv) solve the equations.

2.4. Other numerical methods

DDA, T-matrix, and FDTD are the examples of other numerical methods used to simulate optical properties of nanoparticles; however, all of them have some specific disadvantages that exclude them from being exhaustive and comprehensive.

Some of these disadvantages are presented as follows. The DDA method needs to apply use of a condition in order to have a convergence solution. During computation for flat and lengthy objects, the matrices are shortened therefore T-matrix solutions are not stable for such objects. A much wider frequency range is necessary to specify for the FDTD method, in other words, it computes a broadband response but not for a specific wavelength.

By considering all aspects, it would be more logical to use FEM as a comprehensive numerical method to simulate optical properties of nanoparticles. It does not have any critical disadvantages to restrict its application, and its solutions are the most accurate ones. For FEM, its slightly lengthy computational time can be reduced by a more powerful computer while its response is always precise and equivalent.

3. Discussion

The absorption efficiency of the hollow nanoshells with appropriate dimensions is presented in this paper. The efficiency is placed in the first and second near-infrared regions and compared with other nanoshells. The diagrams clearly show the superiority of using the hollow nanoshells over other nanoshells in both the first and second regions.

3.1. Spherical nanoshells

Nanostructures in the shapes of sphere and spherical shells are widely used in medical applications. Such shapes in 2 and 3 dimensions are shown in Figs. 1 and 2.

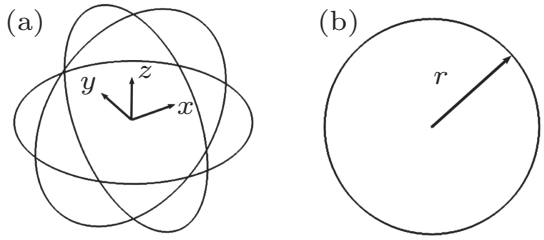


Fig. 1. Schematics of nanospheres with radius r in three (a) and two dimensions (b).

Figure 2 shows the spherical nanoshell which has a core with a radius of r_1 and a shell with a radius of r_2. Thus, the thickness of the gold shell is $t = r_2 - r_1$. In the nanostructure, the core contains a material with a constant refractive index like silica ($n = 1.44$) and gold with a thickness of t covers the core.

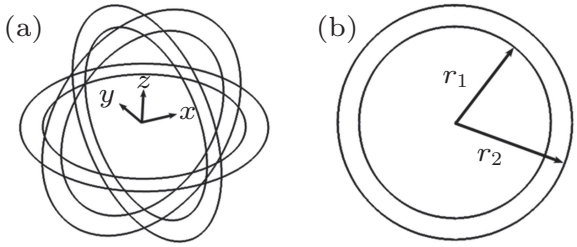


Fig. 2. Schematics of spherical nanoshell with core radius r_1 and shell radius r_2 in three (a) and two dimensions (b).

As mentioned before scattering the absorption efficiencies of gold spherical nanoparticles can be simulated by Mie theory. So in order to show a very high compatibility between Mie theory and FEM for spherical nanostructure some numerical values and simulated diagrams are presented and compared herein.

Table 1 shows the numerical values of absorption and scattering efficiencies of a sphere with radius 40 nm at some different wavelengths, computed by solving Mie theory and the FEM method.

Table 1. Comparison between the computed numerical values of efficiencies for spherical nanoparticles with radius 40 nm at different wavelengths, obtained by Mie theory and FEM.

λ/nm	Q_{abs} Mie	Q_{abs} FEM	Q_{sca} Mie	Q_{sca} FEM
400	2.153206514	2.16×10^{0}	0.8997864799	0.90457
450	2.235753233	2.23×10^{0}	0.7005297957	0.69783
500	2.575689343	2.58×10^{0}	0.7188831486	0.73017
550	3.645651195	3.61×10^{0}	2.817775445	2.80392
600	1.044624564	1.04×10^{0}	1.714225378	1.73094
650	0.2527850675	2.48×10^{-1}	0.7574652125	0.76647
700	0.1077948317	1.07×10^{-1}	0.4107168010	0.41858
750	0.0678623913	6.83×10^{-2}	0.2530165931	0.26086

Figure 3 shows the absorption and scattering efficiencies of such a sphere obtained by solving Mie theory and figure 4 shows the same things achieved by FEM. Figure 5 compares the previous two diagrams with each other. It can be seen from this figure that the FEM is highly compatible with Mie theory. In fact, we can just achieve the absorption efficiencies of a few limited types of nanostructures by using Mie theory while FEM gives us the absorption efficiencies of any different types of nanostructures. Besides, the results of such a limited range of nanostructures obtained by Mie theory are the same as the results obtained by FEM (Fig. 5). So, it would be more logical to use FEM, which is more comprehensive and practical, for all types of nanostructures.

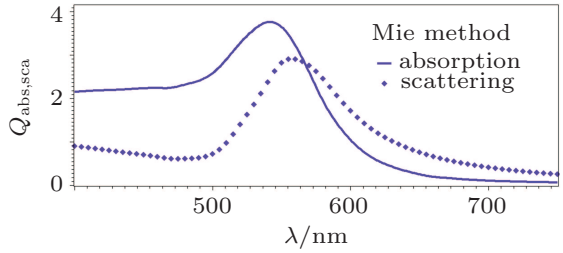


Fig. 3. (color online) Absorption and scattering efficiency spectrum of gold nanosphere with radius 40 nm computed by Mie method.

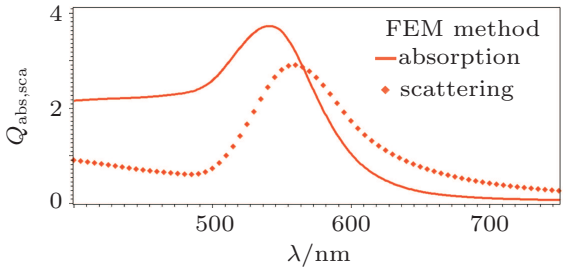


Fig. 4. (color online) Absorption and scattering efficiency spectrum of gold nanosphere with radius 40 nm computed by FEM method.

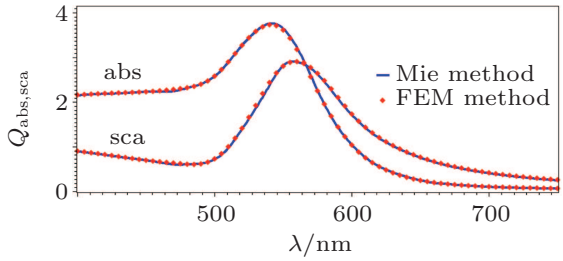


Fig. 5. (color online) Comparison between efficiencies of a sphere with radius 40 nm obtained by Mie theory and FEM method.

As shown in Fig. 6, nanoshells are more appropriate options rather than nanospheres in cancer therapy because the wavelength of maximum absorption is placed in the first near-infrared window and they also have much more fractions of absorption efficiency than nanospheres. It can be seen from the diagrams of absorption efficiency of nanoshells that by increasing the refractive index of the core from 1 to 1.5, the absorption peak height gradually decreases and the peak shifts towards longer wavelengths. Scientists usually use silica–Au nanoshells (with $n = 1.44$ for silica) in order to access more fractions of absorption efficiency and to put the efficiency peak into the near-infrared region. By comparing the absorption efficiencies of nanoshells with different cores in Fig. 6, it is observed that due to the highest absorption efficiency and the absence of inconsistent core with the tissues, the hollow nanoshells with such sizes are the best options in treating the cancerous tissues which are not deep. Therefore, there is no need to use silica nanoshells with toxic cores in medical applications.

Figures 6 and 7 show that by increasing the radius from 20-nm to 40-nm absorption peaks of gold nanospheres are still outside the near-infrared region but absorption peaks of nanoshells are in the second near-infrared window. Thus if we want to eradicate cancerous tissues in the depths of the body, the nanoshells with a shell radius of 40 nm are acceptable options. In nanoshell diagrams, increasing core refractive index leads to the continuous decrease in absorption efficiency and wavelength of maximum absorption shifts to the longer wavelength. Therefore, to eradicate cancerous tissues which are located deep in the body, hollow spherical nanoshells, which have the highest absorption efficiency, are the best options among all nanoshells, which is peculiarly true with silica–Au nanoshells used traditionally in medical applications.

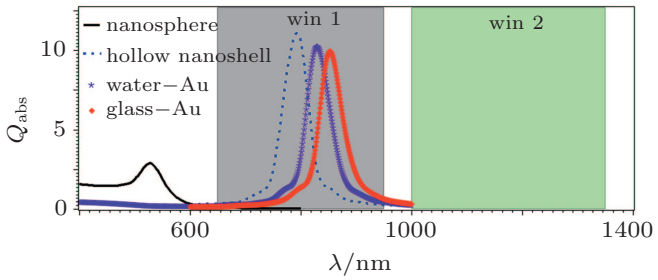


Fig. 6. (color online) Absorption efficiency spectra of gold nanospheres with radius 20 nm and nanoshells with different core materials and radii $r_1 = 18$ nm, $r_2 = 20$ nm.

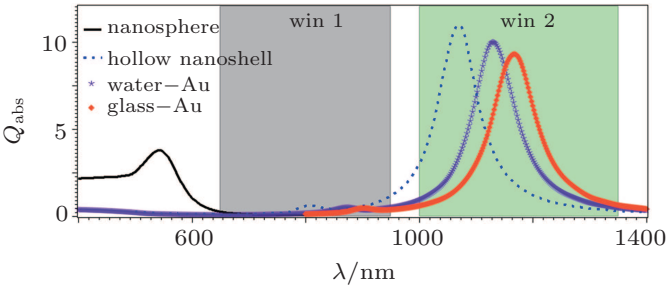


Fig. 7. (color online) Plots of absorption efficiency versus wavelength for gold nanospheres with radius 40 nm and nanoshells with different core materials and radii $r_1 = 38$ nm, $r_2 = 40$ nm.

With respect to other spherical nanoshells which have different core materials, we have hitherto proven the superiority of hollow spherical nanoshells. In the following figures, efficiency diagrams of the hollow nanoshells are drawn in two different cases to examine their optical tunability.

To present a more precise discussion, we have constant thickness and variable radius for the first case, while in the second one, we have variable thickness and constant radius.

In the first case, figure 8 shows that by increasing the shell radius (r_2) from 20 nm to 60 nm, the height of the absorption peak decreases gradually and the peak shifts to a longer wavelength, i.e., from the first window to the second window of near-infrared. If we want to use the hollow nanoshells to eradicate deeper cancerous tissues, we should use nanoshells with a larger shell radius, and if we want to kill the cancerous tissues which are not in the deeper part of body, using nanoshells with a smaller radius is more appropriate.

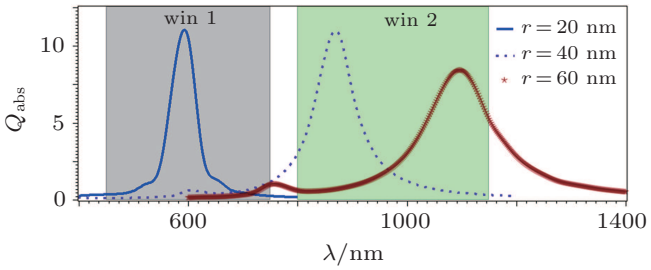


Fig. 8. (color online) Plots of absorption efficiency versus wavelength for hollow nanoshells with different shell radii (r_2) and constant thickness of 2 nm.

In the second case, figure 9 shows that by reducing the thickness from 4 nm to 1 nm, the absorption peak first increases and then decreases. The wavelength of maximum absorption, however, shifts to a higher wavelength, i.e., from the first window into the second window of near-infrared. If need be we can shift the absorption peak into the first or second window by adjusting the thickness of the nanoshells.

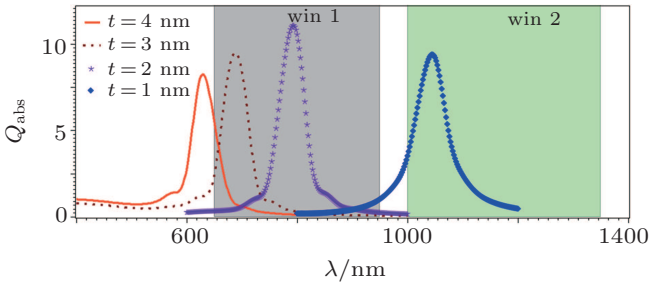


Fig. 9. (color online) Plots of absorption efficiency versus wavelength for hollow nanoshells with shell radius (r_2) of 20 nm and different thickness values.

3.2. Nanotubes

Like Fig. 10, the geometry of nanorods is considered as a cylinder capped with two hemispheres on each side.

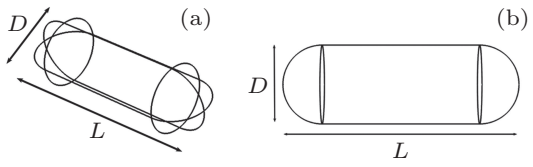


Fig. 10. Schematis of gold nanorod with length L and width D in three (a) and two dimensions (b).

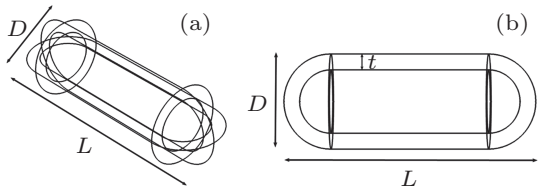


Fig. 11. Schematics of nanotube with length L and width D in three (a) and two dimensions (b).

Nanotubes are rod-shaped nanoshells with a core of constant refractive index which is covered in a gold shell with thickness of t. Figure 11 provides the schematics of the nanotube. If an electromagnetic wave is irradiated onto the nanoparticles in the direction of L, the polarization is called longitudinal polarization and if it is irradiated in the direction of D, the polarization is named transverse polarization.[101]

3.2.1. Longitudinal polarization

Figure 12 shows the spectra of absorption efficiencies for gold nanorods with a diameter of 20 nm and different lengths in the longitudinal polarization. From this figure, we can observe that by increasing the length of nanorod, the peaks of absorption efficiencies shift to longer wavelengths and the efficiencies steadily increase. Thus, if we want to adjust the absorption efficiency of nanorods into the second near-infrared window, the dimensions of nanorods should be larger than 100 nm (as mentioned before this is a disadvantage).

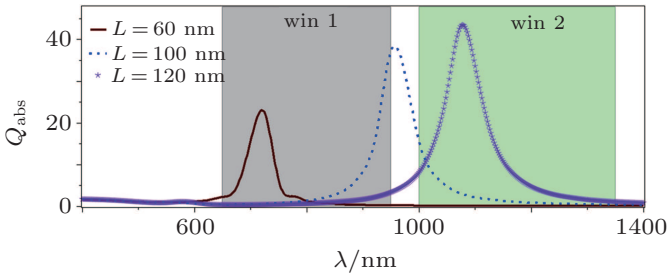


Fig. 12. (color online) Plots of absorption efficiency spectra of nanorods with the same diameter ($D = 20$ nm) and different lengths.

Figure 13 shows that with the same dimensions we can use nanotubes instead of nanorods, which means that without using dimensions greater than 100 nm, eradicating the deep cancerous tissues is feasible. Although in current medical applications, nanorods are widely used, our findings show that it is useful to use nanotubes in necessary circumstances.

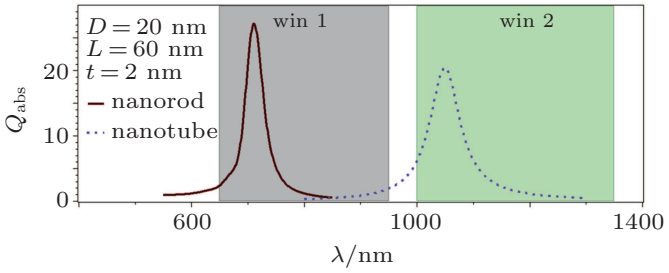


Fig. 13. (color online) Plots of absorption efficiency spectra of nanorods and nanotubes of the same diameter and length, and 2-nm thickness for nanotubes.

Figure 14 shows that by increasing the core refractive index from 1 to 1.5, plasmon peaks shift to longer wavelengths, and the absorption efficiencies decrease. Thus, due to their bigger absorption efficiency, gold nanotubes are more useful for removing tumors than the other nanoshells with different core materials.

In the previous two figures, the superiority of nanotubes with respect to nanorods and other nanoshells with different core materials is observed. Now the optical tunability of gold nanotubes is analyzed in two cases.

To present the discussion more precisely, we have constant thickness and variable length for the first case, but in the second one, we have variable thickness and constant length.

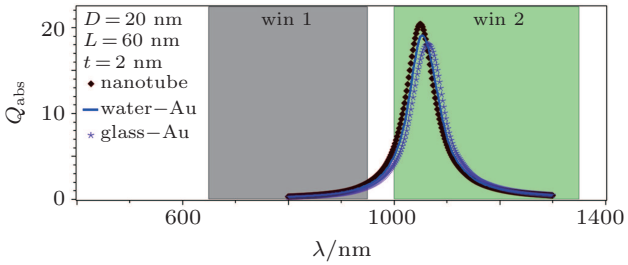


Fig. 14. (color online) Plots of absorption efficiency spectra of gold nanoshells with given dimensions and different core materials.

In the first case, figure 15 shows that by increasing the length from 40 nm to 80 nm, the peaks of absorption efficiencies shift from the first window to the second window of near-infrared and their values increase steadily. Therefore, nanotubes with bigger length can be used in removing tumors in deep tissue.

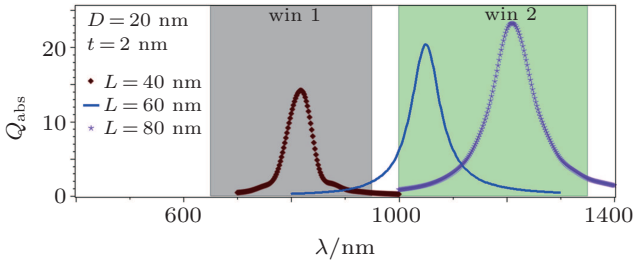


Fig. 15. (color online) Plots of the absorption efficiency spectra of gold nanotubes with the same diameter and thickness and different lengths.

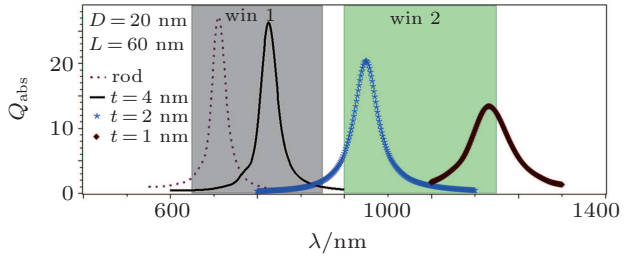


Fig. 16. (color online) Plots of absorption efficiency spectra of gold nanorod and nanotubes with the same dimensions and different thickness values.

In the second case, figure 16 shows that by reducing the thickness from 4 nm to 1 nm, the peaks of absorption efficiencies shift from the first window into the second window of near-infrared and their values decrease steadily. Therefore, by adjusting the nanotube thickness, the plasmon peak can be situated in the first or second region.

3.2.2. Transverse polarization

Figure 17 shows that increasing the length of nanotube does not induce the absorption peaks to shift, but the value of efficiency first decreases and then increases again.

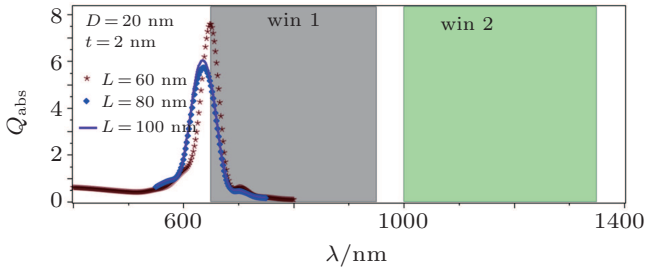


Fig. 17. (color online) Plots of absorption efficiency spectra of nanotubes with the same diameter and thickness and different lengths in the transverse polarization.

Figure 18 shows that by reducing the thickness of nanotube, the absorption efficiencies increase and plasmon peaks enter into the first infrared window.

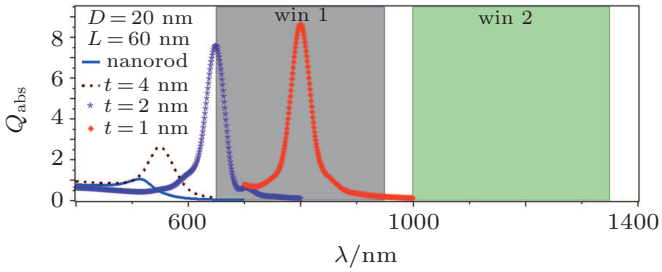


Fig. 18. (color online) Plots of the absorption efficiency spectra of gold nanorod and nanotubes with the same dimension and different thickness values for nanotubes.

By comparing the transverse polarization diagram with the longitudinal polarization diagram, it is seen that the longitudinal polarization is more efficient than the transverse polarization because the plasmon peak will have a bigger absorption efficiency and enters into the second near infrared region. Nevertheless, if we want to use the transverse polarization, using the lesser length and thickness is more acceptable for achieving better efficiency.

4. Conclusions

In order to choose the best core in cancer therapy, the absorption efficiencies of nanoshells with different core materials in different shapes are compared with each other. Performed simulations made us choose the hollow nanoshells as the best option in photothermal therapy (PTT). This is because of the optical tunability, bigger absorption efficiency, the compatible core with body tissues and lower dosage of nanomaterials, which leads to lower cost of treatment.

References

[1] Brannon-Peppas L and Blanchette J O 2012 *Adv. Drug Deliv. Rev.* **64** 206
[2] Yu J, Huang D Y, Yousaf M Z, Hou Y L and Gao S 2013 *Chin. Phys. B* **22** 027506
[3] Jiao P F, Zhou H Y, Chen L X and Yan B 2011 *Curr. Med. Chem.* **18** 2086
[4] Jain S, Hirst D G and O'Sullivan J M 2012 *Br. J. Radiol.* **85** 101
[5] Wang M and Thanou M 2010 *Pharmacol. Res.* **62** 90
[6] Yu M K, Park J and Jon S 2012 *Theranostics.* **2** 3
[7] Kumar A, Ma H, Zhang X, Huang K, Jin S, Liu J, Wei T, Cao W, Zou G and Liang X J 2012 *Biomaterials* **33** 1180
[8] Dreaden E C, Austin L A, Mackey M A and El-Sayed M A 2012 *Ther. Deliv.* **3** 457
[9] Gil P R and Parak W J 2008 *ACS Nano* **2** 2200
[10] Huang X and El-Sayed M A 2011 *Alexandria J. Med.* **47** 1
[11] Glazer E S and Curley S A 2011 *Surg. Oncol. Clin. N. Am.* **20** 229
[12] Yue X L, Ma F and Dai Z F 2014 *Chin. Phys. B* **23** 044301
[13] Shibu E S, Hamada M, Murase N and Biju V 2013 *J. Photochem. Photobiol. C Photochem. Rev.* **15** 53
[14] Dickerson E B, Dreaden E C, Huang X, El-Sayed I H, Chu H, Pushpanketh S, McDonald J F and El-Sayed M A 2008 *Cancer Lett.* **269** 57
[15] Gobin A M, Lee M H, Halas N J, James W D, Drezek R A and West J L 2007 *Nano Lett.* **7** 1929
[16] Melancon M P, Zhou M and Li C 2011 *Acc. Chem. Res.* **44** 947
[17] Choi W Il, Sahu A, Kim Y H and Tae G 2012 *Ann. Biomed. Eng.* **40** 534
[18] Rozanova N and Zhang J 2009 *Sci. China, Ser. B Chem.* **52** 1559
[19] MacKey M A, Ali M R K, Austin L A, Near R D and El-Sayed M A 2014 *J. Phys. Chem. B* **118** 1319
[20] Kirui D K, Krishnan S, Strickland A D and Batt C A 2011 *Macromol. Biosci.* **11** 779
[21] Lu W, Zhang G, Zhang R, Flores L G, Huang Q, Gelovani J G and Li C 2010 *Cancer Res.* **70** 3177
[22] Vijayaraghavan P, Liu C H, Vankayala R, Chiang C S and Hwang K C 2014 *Adv. Mater.* **26** 6689
[23] Ayala-Orozco C, Urban C, Bishnoi S, Urban A, Charron H, Mitchell T, Shea M, Nanda S, Schiff R, Halas N and Joshi A 2014 *J. Control Release* **191** 90
[24] Lu W, Xiong C, Zhang G, Huang Q, Zhang R, Zhang J Z and Li C 2009 *Clin. Cancer Res.* **15** 876
[25] Mallick S, Sun I C, Kim K and Yi D K 2013 *J. Nanosci. Nanotechnol.* **13** 3223
[26] Yin N Q, Liu L, Lei J M, Jiang T T, Zhu L X and Xu X L 2013 *Chin. Phys. B* **22** 097502
[27] Shao J, Griffin R J, Galanzha E I, Kim J W, Koonce N, Webber J, Mustafa T, Biris A S, Nedosekin D A and Zharov V P 2013 *Sci. Rep.* **3** 1293
[28] Khlebtsov N G and Dykman L A 2010 *J. Quantum Spectrosc. Radiat. Transf.* **111** 1
[29] Henry A I, Bingham J M, Ringe E, Marks L D, Schatz G C and Van Duyne R P 2011 *J. Phys. Chem. C* **115** 9291
[30] Major K J, De C and Obare S O 2009 *Plasmonics* **4** 61
[31] Zhang H X, Gu Y and Gong Q H 2008 *Chin. Phys. B* **17** 2567
[32] Rodríguez-Oliveros R and Sánchez-Gil J A 2012 *Opt. Express* **20** 621
[33] Petryayeva E and Krull U J 2011 *Anal. Chim. Acta* **706** 8
[34] Zhang J and Zhang L 2012 *Adv. Opt. Photon.* **4** 157
[35] Hutter E and Fendler J H 2004 *Adv. Mater.* **16** 1685
[36] Mitchell J 2010 *Sensors* **10** 7323
[37] Xie H N, Larmour I A, Smith W E, Faulds K and Graham D 2012 *J. Phys. Chem. C* **116** 8338
[38] Zeng S, Yu X, Law W C, Zhang Y, Hu R, Dinh X Q, Ho H P and Yong K T 2013 *Sensors Actuators B: Chem.* **176** 1128
[39] Olson T Y, Schwartzberg A M, Orme C A, Talley C E, Conneull B and Zhang J Z 2008 *J. Phys. Chem. C* **112** 6319
[40] Klar T, Perner M, Grosse S, von Plessen G, Spirkl W and Feldmann J 1998 *Phys. Rev. Lett.* **80** 4249
[41] Xiang G, Zhang N and Zhou X 2010 *Nanoscale Res. Lett.* **5** 818
[42] Jain P K, Lee K S, El-Sayed I H and El-Sayed M A 2006 *J. Phys. Chem. B* **110** 7238
[43] Wang J, Wheeler D, Zhang J Z, Achilefu S and Kang K A 2013 *Adv. Exp. Med. Biol.* **765** 323
[44] Lee J, Chatterjee D K, Lee M H and Krishnan S 2014 *Cancer Lett.* **347** 46
[45] You J, Zhang R, Zhang G, Zhong M, Liu Y, Van Pelt C S, Liang D, Wei W, Sood A K and Li C 2012 *J. Control Release* **158** 319
[46] Cheng F Y, Chen C T and Yeh C S 2009 *Nanotechnology* **20** 425104
[47] Sikdar D, Rukhlenko I D, Cheng W and Premaratne M 2013 *Nanoscale Res. Lett.* **8** 142
[48] Han J, Li J, Jia W, Yao L, Li X, Jiang L and Tian Y 2014 *ACS Nano* **4** 1033
[49] Guo L, Panderi I, Yan D D, Szulak K, Li Y, Chen Y T, Ma H, Niesen D B, Seeram N, Ahmed A, Yan B, Pantazatos D and Lu W 2013 *ACS Nano* **7** 8780
[50] Jelveh S and Chithrani D B 2011 *Cancers* **3** 1081
[51] Park J, Park J, Ju E J, Park S S, Choi J, Lee J H, Lee K J, Shin S H, Ko E J, Park I, Kim C, Hwang J J, Lee J S, Song S Y, Jeong S Y and Choi E K 2015 *J. Control Release* **207** 77
[52] Almeida J P M, Figueroa E R and Drezek R A 2014 *Nanomed. Nanotech. Biol. Med.* **10** 503
[53] Melancon M P, Lu W, Yang Z, Zhang R, Cheng Z, Elliot A M, Stafford J, Olson T, Zhang J Z and Li C 2008 *Mol. Cancer Ther.* **7** 1730
[54] Chen J, Wang D, Xi J, Au L, Siekkinen A, Warsen A, Li Z Y, Zhang H, Xia Y and Li X 2007 *Nano Lett.* **7** 1318
[55] Khlebtsov N and Dykman L 2011 *Chem. Soc. Rev.* **40** 1647
[56] Dreaden E C, Mackey M A, Huang X, Kang B and El-Sayed M A 2011 *Chem. Soc. Rev.* **40** 3391
[57] Lim Z Z J, Li J E J, Ng C T, Yung L Y L and Bay B H 2011 *Acta Pharmacol. Sin.* **32** 983
[58] Boisselier E and Astruc D 2009 *Chem. Soc. Rev.* **38** 1759
[59] Zhang J Z 2010 *J. Phys. Chem. Lett.* **1** 686
[60] Kennedy L C, Bickford L R, Lewinski N A, Coughlin A J, Hu Y, Day E S, West J L and Drezek R A 2011 *Small* **7** 169
[61] Alkilany A M, Thompson L B, Boulos S P, Sisco P N and Murphy C J 2012 *Adv. Drug Deliv. Rev.* **64** 190
[62] Krishnan S R and George S K 2014 *Pharmacology and Therapeutics*, 8th edn. (Europe: InTech) pp. 235–253
[63] Huang X, Jain P K, El-Sayed I H and El-Sayed M A 2008 *Lasers Med. Sci.* **23** 217
[64] Wang Y, Black K C L, Luehmann H, Li W, Zhang Y, Cai X, Wan D, Liu S Y, Li M, Kim P, Li Z Y, Wang L V, Liu Y and Xia Y 2013 *ACS Nano* **7** 2068
[65] Khlebtsov B, Zharov V, Melnikov A, Tuchin V and Khlebtsov N 2010 *Nanotechnology* **17** 5167
[66] Hong G, Robinson J T, Zhang Y, Diao S, Antaris A L, Wang Q and Dai H 2012 *Angew. Chemie Int. Ed.* **51** 9818
[67] Yasun E, Kang H, Erdal H, Cansiz S, Ocsoy I, Huang Y F and Tan W 2013 *Interface Focus* **3** 20130006
[68] Smith A M, Mancini M C and Nie S 2009 *Nat. Nanotechnol.* **4** 710
[69] Welsher K, Sherlock S P and Dai H 2011 *Proc. Natl. Acad. Sci. USA* **108** 8943
[70] Sun Y, Mayers B and Xia Y 2003 *Adv. Mater.* **15** 641
[71] Abdollahi S N, Naderi M and Amoabediny G 2013 *Colloids Surfaces A: Physicochem. Eng. Asp.* **436** 1069
[72] Zhou L, Yu X F, Fu X F, Hao Z H and Li K Y 2008 *Chin. Phys. Lett.* **25** 1776
[73] Vongsavat V, Vittur B M, Bryan W W, Kim J H and Lee T R 2011 *ACS Appl. Mater. Interfaces* **3** 3616
[74] Zhong X, Chai Y Q and Yuan R 2014 *Talanta* **128** 9
[75] Liang Z, Susha A and Caruso F 2003 *Chem. Mater.* **15** 3176
[76] Cheng K and Sun S 2010 *Nano Today* **5** 183
[77] Ma L N, Liu D J and Wang Z X 2010 *Chin. J. Anal. Chem.* **38** 1
[78] Fan H J, Gosele U and Zacharias M 2007 *Small* **3** 1660
[79] Xie H, Larmour I A, Chen Y C, Wark A W, Tileli V, McComb D W, Faulds K and Graham D 2013 *Nanoscale* **5** 765
[80] Song C, Zhao G, Zhang P and Rosi N L 2010 *J. Am. Chem. Soc.* **132** 14033
[81] An K and Hyeon T 2009 *Nano Today* **4** 359
[82] Lou X W, Archer L A and Yang Z 2008 *Adv. Mater.* **20** 3987
[83] Parsons J, Burrows C P, Sambles J R and Barnes W L 2010 *J. Mod. Opt.* **57** 356
[84] Van De Hulst H C 1981 *Light Scattering by Small Particles* (New York: Dover)

[85] Mie G 1908 *Ann. Phys.* **25** 377
[86] Bohren C F and Huffman D R 1983 *Absorption and Scattering of Light by Small Particles*, Vol. 1 (New York: Wiley and Sons, Inc.)
[87] Wriedt T 2012 *Mie theory: A review. Springer Ser. Opt. Sci.* **169** 53
[88] Quinten M 2011 *Optical Properties of Nanoparticle Systems: Mie and Beyond* (New York: Wiley)
[89] Hergert W and Wriedt T 2012 *The Mie Theory: Mie Theory Basics Appl*. pp. 53–71
[90] Papoff F and Hourahine B 2011 *Opt. Express* **19** 21432
[91] Xu H X 2003 *Phys. Lett. Sect. A: Gen. At. Solid State Phys.* **312** 411
[92] Salandrino A, Fardad S and Christodoulides D N 2012 *J. Opt. Soc. Am. B* **29** 855
[93] Zienkiewicz O C, Taylor R L and Zhu J Z 2013 *Finite Element Method its Basis Fundam*. pp. 493–543
[94] Morgan K, Hassan O and Weatherill N P 1981 *The Finite Element Method*, Acad. Eng. Polish, Acad. Sci. Chin., Acad. Sci. Natl. Acad. Sci. Italy (Academia dei Lincei) 35 110
[95] Nikishkov G 2004 "Introduction to the finite element method", University Aizu, pp. 1–70
[96] Polyanskiy M N 2016 Refractive index database, http://refractiveindex.info
[97] Jianming J 2002 *The Finite Element Method in Electromagnetics*, 2nd edn. (Urbana-Champaign: Wiley-IEEE Press)
[98] Volakis J L, Chatterjee A and Kempel L C 1998 *Finite element method for electro-magnetics: antennas, microwave circuits, and scattering applications* (Ann Arbor: Wiley-IEEE Press)
[99] Monk P 2003 *Finite element methods for Maxwell's equations* (Oxford: Oxford University Press)
[100] Davletshin Y 2010 *Modeling the optical properties of a single gold nanorod for use in biomedical applications* (Toronto: Ryerson University) pp. 10–35
[101] Wang S, Xu H and Ye J 2014 *Phys. Chem.* **16** 12275